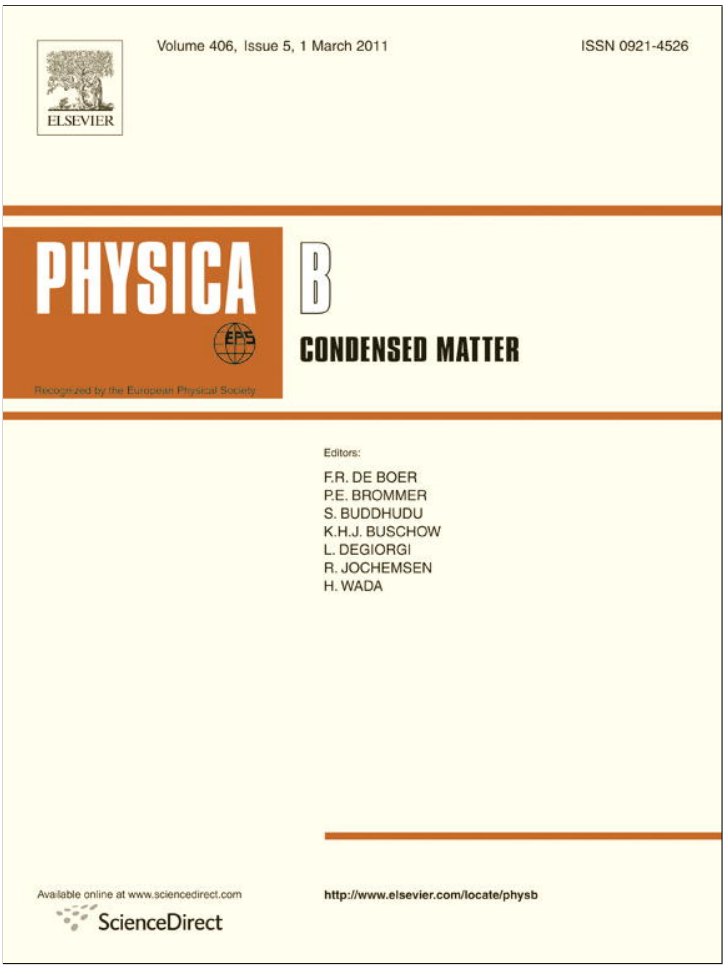

Physica B 406 (2011) 1132–1138

Contents lists available at ScienceDirect

Physica B

journal homepage: www.elsevier.com/locate/physb

Dynamics and order–disorder transitions in bidisperse diblock copolymer blends

Yueqiang Wang, Xuan Li, Ping Tang*, Yuliang Yang

Key Laboratory of Molecular Engineering of Polymer, Ministry of Education, Department of Macromolecular Science, Fudan University, Shanghai 200433, China

ARTICLE INFO

Article history:
Received 22 November 2010
Received in revised form
26 December 2010
Accepted 28 December 2010
Available online 1 January 2011

Keywords:
Dynamic self-consistent field theory (DSCFT)
Order–disorder transitions (ODT)
Polydispersity index (PDI)
Variable cell shape

ABSTRACT

We employ the dynamic extension of self-consistent field theory (DSCFT) to study dynamics and order–disorder transitions (ODT) in AB diblock copolymer binary mixtures of two different monodisperse chain lengths by imitating the dynamic storage modulus G′ corresponding to any given morphology in the oscillatory shear measurements. The different polydispersity index (PDI) is introduced by binary blending AB diblock copolymers with variations in chain lengths and chain number fractions. The simulation results show that the increase of polydispersity in the minority or symmetric block introduces a decrease in the segregation strength at the ODT, $(\chi N)_{ODT}$, whereas the increase of polydispersity in the majority block results in a decrease, then increase and final decrease again in $(\chi N)_{ODT}$. To the best of our knowledge, our DSCFT simulations, for the first time, predict an increase in $(\chi N)_{ODT}$ with the PDI in the majority block, which produces the experimental results. The simulations by previous SCFT, which generally speaking, is capable of describing equilibrium morphologies, however, contradict the experimental data. The polydispersity acquired by properly tuning the chain lengths and number fractions of binary diblock copolymer blends should be a convenient and efficient way to control the microphase separation strength at the ODT.

1. Introduction

Due to microphase separation, block copolymers in melts and solutions can self-assemble into a variety of ordered structures such as lamellae (LAM), hexagonally packed cylinders (HEX), and body centered cubic (BCC) spheres and more complex structures such as gyroid (G) [1]. The specific phase behaviors are largely governed by two parameters: the volume fraction or composition of the block f and the degree of phase separation between unlike segments χN, which is the product of the total number-average of segments N and the effective Flory–Huggins interaction parameter χ. In the past decades, much attention has been focused both experimentally and theoretically on explaining complexity and underlying physical phenomena in self-assembly and morphology of monodisperse block copolymers with polydispersity indices (PDI$=M_w/M_n$) of 1. In fact, most experimental researches on block copolymers have concentrated on macromolecules with nearly monodispersity prepared by living anionic polymerization technique. However, polydispersity effects in chain lengths have become increasingly important as synthetic techniques such as controlled radical polymerization (CRP), which are now offering more economical ways of synthesizing block copolymers but generally result in some certain degree of polydispersity compared to traditional anionic polymerization technique [2,3]. Furthermore, inevitable polydispersity may have potential implications on the processability and advantageous properties of block copolymers. For instance, by properly tuning the PDI, the segregation strength at the order–disorder transitions (ODT), $(\chi N)_{ODT}$ (inversely proportional to the temperature) is changed conveniently and thus the favorable processing temperature can be obtained. To make use of this fact, it is important to investigate and understand how the polydispersity affects the known behavior of monodisperse systems.

The research on the effect of the PDI on the phase behavior of diblock copolymers recently has been concluded in a review [4]. Most experimental and theoretical investigations have focused on the influence of polydispersity on the morphology as well as morphological transitions. Matsushita et al. prepared a series of diblock copolymer systems with controlled PDI of PS block by mixing several relatively monodisperse samples. They found that polydispersity increased the lamellae period, and at sufficiently high polydispersity, macrophase separation occurred producing coexistence between a well-ordered lamellae microstructure and some poorly ordered morphologies [5]. Lynd and Hillmyer [6] and Lynd et al. [7] found that polydispersity in the A block caused a significant increase in the domain spacing, similar to the experiments by Matsushita et al. [5]. They also found that increase in PDI in the minority component led to a morphology change to one with larger mean interfacial curvature, whereas PDI increase in the majority component resulted in the morphology with smaller

* Corresponding author. Fax: +86 21 65642867.
E-mail address: pingtang@fudan.edu.cn (P. Tang).

0921-4526/$ - see front matter © 2010 Elsevier B.V. All rights reserved.
doi:10.1016/j.physb.2010.12.066

mean interfacial curvature. Recently, Meuler et al. [8] extended the study on the effect of polydispersity of terminal and middle bridged blocks on the morphology and the ODT in poly(isoprene-b-styrene-b-ethylene oxide) triblock terpolymers. These experimental results have been confirmed by theoretical work [9–12].

Self-consistent field theory (SCFT) has been successful in predicting the equilibrium self-assembled morphologies of complex multiblock copolymers in bulk [13,14], due to the development of real-space implementation of SCFT by Drolet and Fredrickson [15]. However, there is notable discrepancy in polydispersity effect on the ODT between SCFT and experiments. For example, Lynd and Hillmyer experimentally found that increase in PDI in the minority component resulted in a decrease in $(\chi N)_{\mathrm{ODT}}$, whereas increase in PDI in the majority component led to an increase in $(\chi N)_{\mathrm{ODT}}$ [16]. However, traditional SCFT predicted a decrease in $(\chi N)_{\mathrm{ODT}}$ with PDI at all copolymer compositions for AB diblock copolymers [10–12]. Recently, morphological transition of polydispersed ABA triblock copolymers has been studied with RPA and static SCFT by Meuler et al. who also found that polydispersity led to stability of ordered structures [8]. Matsen employed the Monte Carlo simulation to study the effects of polydispersity on the order–disorder transition of diblock copolymer melts, indicating that a relatively small shift in the ODT at symmetrical composition, which has reached agreement with the experiment far better than traditional SCFT results [9]. He did not investigate, however, asymmetric composition especially when the majority component is polydisperse [17]. In this case, notable inconsistency is found between traditional SCFT simulations and the experiment. Furthermore, SCFT is also inconsistent with Monte Carlo simulations of polydisperse polymers, which so far agree with the experiment [9].

In contrast to equilibrium microphase morphologies of block copolymers, the behavior of block copolymer melts out of equilibrium such as under shear is not fully understood [18]. Narayanan et al. combined SCFT with Brownian dynamics to study the dynamics and rheology of inhomogeneous polymer blends and their interfaces [19]. A dynamic variant of mean-field theory known as DSCFT proposed by Fraaije, combining the generalized time-dependent Landau–Ginzburg (TDGL), has been demonstrated to be a powerful method to describe the mesoscopic dynamics of inhomogeneous polymeric system. This method allows one to investigate the morphology and dynamic characteristics of block copolymers with different architectures under flow [20,21]. Unfortunately, the stress and strain variables were not included in their model. On the other hand, the introduction of strain field in the SCFT with so-called variable cell shape technique proposed by Barrat et al. allows one to investigate the mechanical properties for inhomogeneous block copolymers [22]. In our previous paper [18], we combined variable cell shape method [22] with DSCFT and extended to simulate the rheological measurements for block copolymers. We calculated the storage modulus G' as a function of segregation strength χ, which can be used to study the ODT behavior of block copolymer melts [18]. In fact, rheological measurements appear to be desirable and sensitive tools to identify the ODT and order-to-order transition in contrast to morphology transitions. In this paper, we adopt the above mentioned modified DSCFT approach to study ODT behavior of binary AB diblock copolymer blend melts with bidisperse chain length. Compared to the continuous distribution of polymer chain length, obtaining polydispersity by blending nearly monodisperse block copolymers with different chain lengths is a convenient and controllable strategy. Some experiments have utilized this blending way to investigate the effects of polydispersity on the morphology [23,24]. Recently we investigated the aggregation behavior of polydisperse AB diblock copolymers in solution by simply blending two polymer chains to artificially make the polydispersity [25]. Furthermore, this simplified model is able to account for the individual contribution of each polymer chain to the bulk modulus G', in which we are able to systematically explore the chain length effect of polydispersity on $(\chi N)_{\mathrm{ODT}}$.

2. Theoretical method

To quantitatively elucidate, in polydisperse copolymers, the dynamics and ODT transitions according to long and short chain lengths, the intuitive and efficient way is realized by mixing two block copolymers with different chain lengths. Consider AB diblock copolymers of volume V, containing n Gaussian chains with two different chain lengths, i.e., bidisperse chain length. In this work, for clarity, the bidisperse block copolymer blends are obtained by mixing only two kinds of different chains of which A block lengths are different but B block lengths are the same, denoted by A_1B and A_2B diblock copolymers, respectively. We further assume that A_1B with longer A block length consists of $N_1=N_{A1}+N_B$, and A_2B with shorter A block length consists of $N_2=N_{A2}+N_B$ segments, with each segment having equal statistical segment length b. $\overline{N}=N_1p_1+N_2p_2$ is the average chain length of block copolymer blends, with the chain number fraction p_1 for A_1B and $p_2(p_2=1-p_1)$ for A_2B, respectively. The average compositional volume fractions of species A in binary copolymer blends is $\bar{f}_A=(N_{A1}p_1+N_{A1}p_2)/(N_1p_1+N_2p_2)=(N_{A1}p_1+N_{A2}p_2)/\overline{N}$ ($f_{A1}=N_{A1}p_1/\overline{N}$ and $f_{A2}=N_{A2}P_2/\overline{N}$) and $f_B=1-f_A$. The PDI of the polydisperse block A can be obtained by the formula $\mathrm{PDI}_A=(N_{A1}^2p_1+N_{A2}^2p_2)/(\bar{f}_A\overline{N})^2$.

In order to simulate non-equilibrium microphase separation kinetics under shear for complex architecture block copolymers, the time-dependent Ginzburg–Landau (TDGL) is combined with the SCFT, known as the DSCFT to describe the dynamics of inhomogeneous system. The DSCFT combined with variable cell shape algorithm under shear was described in detail in our previous study [18], which has been successful in dealing with the dynamics and rheology of diblock copolymer blends. The characteristic of this method is capable of accounting for the inhomogeneity-induced changes in the chain conformation and their coupling with the shear through the chain propagator $q(\boldsymbol{r},s)$. We only briefly review the extension of this method to AB diblock copolymers with different chain lengths.

Under shear, the calculation cell can be conveniently described by the so-called variable cell shape method proposed by Barrat et al. [22]. The variable shape cell is described by a 2×2 shape matrix $\boldsymbol{h}$ in 2D ($\mathbf{h}=\begin{vmatrix} h_{xx} & h_{yx} \\ h_{xy} & h_{yy} \end{vmatrix}=\begin{vmatrix} L_x & L_y\cos\alpha \\ 0 & L_y\sin\alpha \end{vmatrix}$ for 2D $L_x\times L_y$ cell, where L_x and L_y are side lengths of the cell and α is the angle between adjacent sides) to hold all the points $\boldsymbol{R}$ in Cartesian coordinates expressed as $\boldsymbol{R}=\boldsymbol{hx}$, where $\boldsymbol{x}$ is a rescaled vector whose components lie in [0,1]. Integrals on $\boldsymbol{R}$ can be converted into integrals over $\boldsymbol{x}$ by using a scaling factor $\det\mathbf{h}$ ($\det\mathbf{h}=V$) representing the volume of the calculation cell. A metric tensor constructed by $\boldsymbol{G}=\boldsymbol{h}^T\boldsymbol{h}$ is used to transform dot products from original Cartesian to rescaled coordinates. Thus, individual AB diblock copolymer chain $q_i(\boldsymbol{x},s)$, where $i=1$ and 2, respectively, represents A_1B and A_2B diblock copolymers, is given by

$$\frac{\partial q_i}{\partial s}=\begin{cases} R_g^2(\mathbf{G}^{-1})_{\alpha\beta}\frac{\partial^2 q_i(\mathbf{x},s)}{\partial x_\alpha \partial x_\beta}-\left[\gamma_A(s)\omega_A(\mathbf{x},s)+\gamma_B(s)\omega_B(\mathbf{x},s)\right] \\ \quad\times q_i(\mathbf{x},s), \quad 0<s<N_{A_i}/\overline{N} \\ R_g^2(\mathbf{G}^{-1})_{\alpha\beta}\frac{\partial^2 q_i(\mathbf{x},s)}{\partial x_\alpha \partial x_\beta}-\left[\gamma_A(s)\omega_A(\mathbf{x},s)+\gamma_B(s)\omega_B(\mathbf{x},s)\right] \\ \quad\times q_i(\mathbf{x},s), \quad N_{A_i}/\overline{N}<s<N_i/\overline{N} \end{cases} \tag{1}$$

with the initial condition $q_i(\mathbf{x},0)=1$, where $R_g^2=\overline{N}b^2/6$ is Gaussian radius of gyration of the chain with length $\overline{N}$, α and β stand for two orthogonal coordinates in original Cartesian, ω_I is the self-consistent field exerted to the species A or B, and $\gamma_I(s)$ is 1 if s belongs to block I and otherwise 0. Because the two ends of diblock chains are distinct, a second end-segment distribution function $q_i^+(\mathbf{x},s)$ is needed that can be similarly obtained with the right side of Eq. (3) multiplied by -1, subjected to the initial condition $q_i^+(\mathbf{x},N_i/\overline{N})=1$. The density of diblock copolymers is thus obtained by

$$\phi_A(\mathbf{x})=\frac{V\overline{N}}{Q_1N_1}\int_0^{N_{A1}/\overline{N}}dsq_1(\mathbf{x},s)q_1^+(\mathbf{x},s)+\frac{V\overline{N}}{Q_2N_2}\int_0^{N_{A2}/\overline{N}}dsq_2(\mathbf{x},s)q_2^+(\mathbf{x},s)$$
$$\phi_B(\mathbf{x})=\frac{V\overline{N}}{Q_1N_1}\int_{N_{A1}/\overline{N}}^{N_1/\overline{N}}dsq_1(\mathbf{x},s)q_1^+(\mathbf{x},s)+\frac{V\overline{N}}{Q_2N_2}\int_{N_{A2}/\overline{N}}^{N_2/\overline{N}}dsq_2(\mathbf{x},s)q_2^+(\mathbf{x},s) \quad (2)$$

where $Q_i=\int d\mathbf{x}q_i(\mathbf{x},N_i/\overline{N})$ is the partition function of the single chain.

Once the chain propagator is obtained, the elastic stress for AB diblock copolymer can be written as [13,22]

$$\frac{\sigma_{\alpha\beta}}{(n/V)k_BT}=\sum_{i=1}^{2}\frac{p_i\times R_g^2}{Q_i}h_{\gamma\alpha}^{-1}h_{\delta\beta}^{-1}\int d\mathbf{x}\left(\int_0^{N_i/\overline{N}}dsq_i(\mathbf{x},s)\frac{\partial^2q_i^+(\mathbf{x},s)}{\partial x_\alpha\partial x_\beta}+\int_0^{N_i/\overline{N}}dsq_i^+(\mathbf{x},s)\frac{\partial^2q_i(\mathbf{x},s)}{\partial x_\alpha\partial x_\beta}\right) \quad (3)$$

The free energy functional is thus given by

$$F=(1/V)\int d\mathbf{x}[\chi_{AB}\overline{N}\phi_A(\mathbf{x})\phi_B(\mathbf{x})-\omega_A\phi_A(\mathbf{x})-\omega_B\phi_B(\mathbf{x})-\xi(1-\phi_A(\mathbf{x})-\phi_B(\mathbf{x}))]-P_1\ln Q_1/V-P_2\ln Q_2/V+\beta V(\boldsymbol{\sigma}:\boldsymbol{\varepsilon}) \quad (4)$$

where the last term in Eq. (4) is the contribution of stress $\boldsymbol{\sigma}$ and strain $\boldsymbol{\varepsilon}$ to the free energy for an incompressible triblock copolymer melt confined to a cell of variable shape, where the strain is given by $\boldsymbol{\varepsilon}=\frac{1}{2}\left[(\mathbf{h}_0^T)^{-1}\mathbf{G}(\mathbf{h}_0)^{-1}-1\right]$, $\boldsymbol{h}_0$ is the original cell shape of the simulation box before deformation.

According to the calculated stress in Eq. (3), the storage modulus G' and loss modulus G'' in traditional oscillatory shear tests can be derived by linear fitting the simulated stress–strain curve as follows:

$$\sigma_{\alpha\beta}=\Gamma[G'\sin(\omega t)+G''\cos(\omega t)] \quad (5)$$

where Γ is the strain amplitude. The microphase separation process of block copolymers is decoupled with rheological measurements to avoid possible effect of shear on the morphology evolution, and thus $G''=0$. The storage modulus, therefore, can be obtained by analyzing the stress–strain relation, i.e., $G'=\sigma_{\alpha\beta}/[\sin(\omega t)\Gamma]$ [18,26,27]. Details of the numerical solution of the above DSCFT equations under rheological measurements refer to our previous paper [18].

3. Results and discussion

In order to investigate the effect of polydispersity of copolymers on the dynamics, for convenience, in this work, polydispersity is obtained by blending binary diblock copolymers differing in chain lengths. The advantage of this idea is available to distinguish individual contributions from different chain lengths, and thus magnifying certain chain length effects. Furthermore, quantitative analysis of mechanical properties can be applied to dynamically detect possible changes in the modulus of the mesophase as polydispersity increases compared with traditional SCFT calculations. As stated in our previous paper [18], temperature sweep of storage modulus G' is employed to investigate the ODT of block copolymers. In our simulations, temperature sweep is implemented by continuously slowly decreasing the Flory–Huggins interaction parameter χ at which phase separation evolves to equilibrium states. Subsequent rheological measurements are carried out at fixed strain amplitude $\Gamma=0.01$ and reduced frequency $\omega=0.02$ ensuring linear viscoelasticity. G' as a function of χ is thus obtained. χ at which the slope of curve G' vs. χ abruptly changes is labeled as χ_{ODT} and the corresponding temperature is T_{ODT}. In addition, the extremely slow change in rate of χ such as $\Delta\chi/t=0.001/1000$ is chosen in our simulations to ensure that each tested morphology is in near equilibrium under corresponding phase segregation conditions. We should note that variable cell shape SCFT is carried out to obtain the equilibrium morphology before rheological measurements implemented with DSCFT.

Due to the unbearable time consumption in 3D calculation, the variable cell shape SCFT simulations are carried out in 2D 36×36 square lattice (the original cell shape of the simulation box) with the grid size of $\Delta x=\Delta y=0.25\,R_g$. We note that the traditional treatment of periodical conditions under shear becomes convenient due to the introduction of the shape matrix for the variable shape cell. In the case of simple shear, the velocity direction is assumed along the x direction and thus $v_x=\Gamma y\omega\cos\omega t$ and $v_y=0$ for externally imposed oscillatory shear flow. The reduced strain γ is the deformation scaled by the original box size. When shear is imposed within one integral multiple deformation of the box size, Eqs. (1) and (3) with Laplacian operator are solved in deformed cells. The beveled horizontal component of cell shape matrix becomes $h_{yx}'=h_{xx}\times\gamma$ accordingly. Then we stop shear when the strain is again increased to the box size, $h_{yx}'/h_{xx}=1$, i.e., the beveled horizontal element of cell shape matrix becomes $h_{yx}'=h_{xx}\times1$ while the other matrix components are kept unchanged. The data $\omega_I'(\mathbf{r}',\gamma)$ and $\phi_I'(\mathbf{r}',\gamma)$ on the rescaled coordinate (x',y') are transformed to $(x'-L_x,y)$ for $L_x\le x'\le2L_x$ and thus $\boldsymbol{h}'$ is back to orthogonal coordinate again. Then restart the shear by using the updated data ω_I and ϕ_I as the next initial values and continue to deform the new cell. When the strain is again increased to the box size, the above described coordinate transformation will be done. The periodical boundary condition under shear is thus implemented by such iteration steps. For simplicity, the average chain length is fixed as $\overline{N}=100$. Therefore, N_1 and p_1, N_2 and p_2 can be chosen with arbitrary numbers to satisfy $\overline{N}=N_1p_1+N_2p_2$. In this case, binary blends are obtained at fixed average chain length $\overline{N}$, but with a distribution in the composition of the constituent chains.

3.1. Effect of PDI on $(\chi N)_{ODT}$ with equal blending number fraction $p_1=p_2=0.5$

At first we consider bidisperse binary AB diblock copolymer blends with equal blending numbers of two kinds of chain lengths, that is, $p_1=p_2=0.5$. The effect of PDI on the ODT is investigated for the fixed average composition of the blends at $\bar{f}_A=0.36$, $\bar{f}_A=0.5$ and $\bar{f}_A=0.64$. Fig. 1 presents the temperature sweep of G' during heating (changes in Flory–Huggins interaction parameters from $\chi=0.16$ to 0.05) for symmetric AB diblock copolymers ($\bar{f}_A=0.5$) with variation in PDI_A in a range from $PDI_A=1$ to 1.81. Order–disorder temperature (T_{ODT}) is identified by a precipitous drop in low-frequency storage modulus G' over a small temperature increment. We can infer from Fig. 1 that the phase segregation degree at the ODT for monodisperse AB diblock copolymers (PDI=1.00) is $\chi_{ODT}=0.105$ at $f_A=0.5$ with average

chain length $N=100$, which is consistent with the theoretical predictions of $\chi N=10.5$ for symmetric diblock copolymers with $f_A=0.5$ [14]. Then continuous increase in PDI leads to the χ_{ODT} shift from $(\chi N)_{ODT}=10.5$ to 7.5. This is in qualitative agreement with mean-field theory predictions and experiments, in which the $(\chi N)_{ODT}$ decreases with increase in PDI at symmetric compositions ($\bar{f}_A=0.5$) [10,11,16,28–30].

Fig. 2 shows the calculated $(\chi N)_{ODT}$ values vs. PDI_A for polydisperse A block with typical compositions of $\bar{f}_A=0.36$, $\bar{f}_A=0.5$ and $\bar{f}_A=0.64$. It is shown that the $(\chi N)_{ODT}$ decreases as PDI_A increases at $\bar{f}_A=0.36$ and $\bar{f}_A=0.5$. In particular, the slopes of lines by linearly fitting the data are negative, and the slopes become less pronounced as the volume fraction of polydisperse A block increases from minority $\bar{f}_A=0.36$ to symmetric composition $\bar{f}_A=0.5$. The result is consistent with previous experiments by Lynd and Hillmyer [16]. and by Meuler et al. [8]. Compared to the monodisperse block copolymers, for polydisperse block copolymers, the longer chains can be less extended to the center of the microphase-separated domain to decrease entropic penalty of stretching, whereas the short chains located at the interface can minimize unfavorable contacts between unlike segments. Therefore, the effect of polydispersity due to long and short chains can fill the space efficiently, resulting in the system to more readily order at lower free energy, i.e., lower $(\chi N)_{ODT}$ relative to the homogeneous disordered state. In other words, polydispersity leads to the elevated temperature required to obtain a disordered state compared to the monodisperse case because $(\chi N)_{ODT}$ is inversely proportional to the temperature T_{ODT}. In fact, the decrease in entropic stretching penalty is also reflected in the increased domain periodicity by previous experiments and SCFT calculations [8,10–12,16,31].

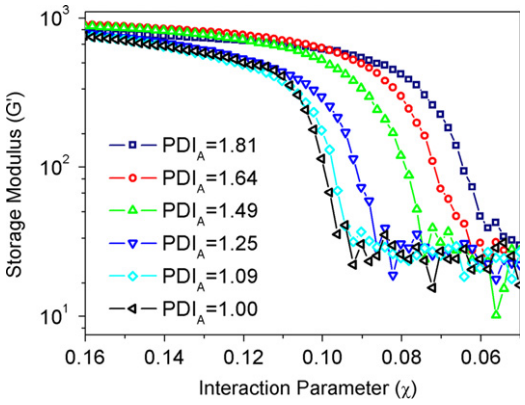

Fig. 1. Simulated temperature sweep of G' (in units of nK_BT/V) for polydisperse A block of symmetric composition AB diblock ($\bar{f}_A=0.5$) blends with equal number fraction ($p_1=p_2=0.5$). The rheological measurement is carried out at strain amplitude $\Gamma=0.01$ and reduced frequency of $\omega=0.02$.

It is interesting to note that in Fig. 2c, the increased $(\chi N)_{ODT}$ values with PDI of the majority block A at certain ranges ($1.4<PDI_A<1.7$) are deviated from the fit line. Lynd and Hillmyer [16] also reported that increase in the polydispersity in the majority component resulted in an increase of $(\chi N)_{ODT}$ by carrying out rheological measurements for controlled polydispersity block copolymers. They speculated that increase in PDI in the majority domain weakens the effective potential holding the phase-separated microdomains ordered in the equilibrium lattice positions, and brings the system close to an entropically favored disordered state. This is similar to the case of block copolymer micelles ordered on a lattice. The increase in polydispersity of the corona blocks will decrease the entropy penalty driving a micelle from its equilibrium position. In this case, the greater number of short chains in the corona readily accommodates a random displacement [32]. Therefore, the strength of the potential holding ordered micelles decreases, resulting in disordered micellar

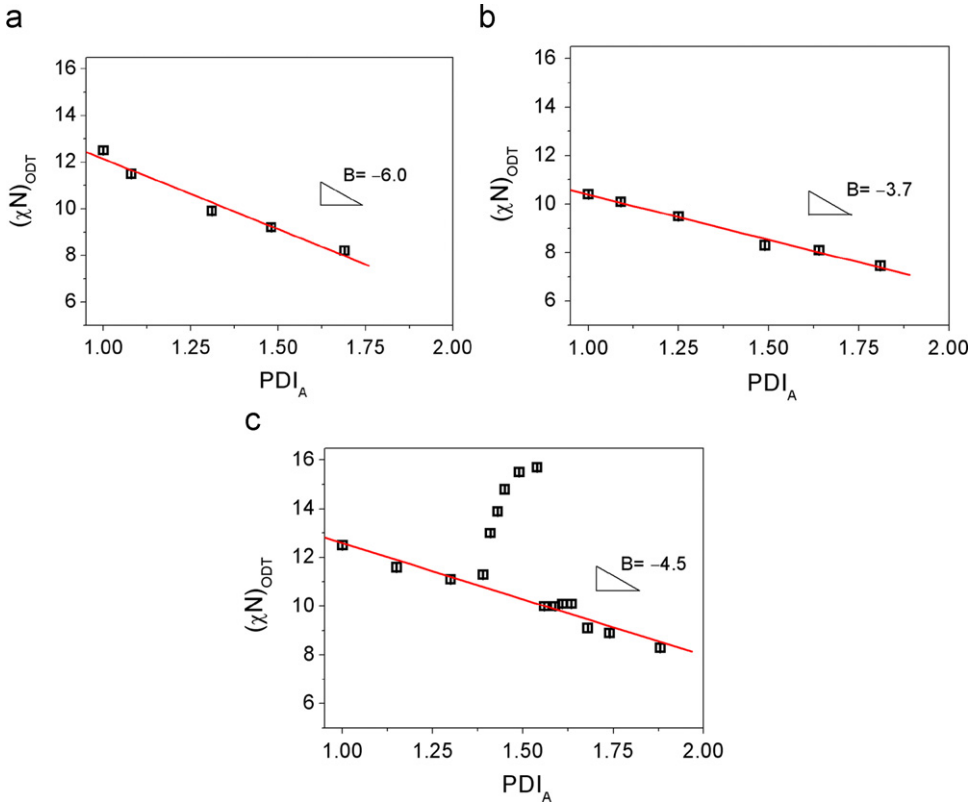

Fig. 2. Simulated $(\chi N)_{ODT}$ vs. PDI_A with equal blending number fraction ($p_1=p_2=0.5$): (a) $\bar{f}_A=0.36$, (b) $\bar{f}_A=0.5$ and (c) $\bar{f}_A=0.64$. The solid lines are linearly fit to the data. In Fig. 2(c), the data in the range from $PDI_A=1.40$ to 1.55 deviated from linear fit are excluded in the fit.

state favoring entropy and the increased $(\chi N)_{ODT}$ as the PDI increases in the majority component. However, the result is disagreement with previous SCFT calculations, which predict that $(\chi N)_{ODT}$ decreases as PDI is increased for all compositions of the polydispersed component [10–12]. As pointed out by Meuler et al., the SCFT simulations may fail to predict the phase behavior at the ODT without accounting for fluctuations [8]. Our DSCFT method in this paper used for simulating rheological measurements appears to be a sensitive tool to identify dynamics and ODT.

3.2. Effect of PDI on $(\chi N)_{ODT}$ with blending random number fraction

Fig. 3 presents the ODT behavior for polydispersed A block of AB diblock binary blends with blending random number fraction p_1 (the number of long chain is not equal to that of the short one). $(\chi N)_{ODT}$ decreases as the PDI increases in the minority at $\bar{f}_A = 0.36$ or symmetric block at $\bar{f}_A = 0.5$. Furthermore, the slopes of lines by linear fit are negative, and the slopes become less pronounced as the volume fraction of polydispersed A block increases from minority $\bar{f}_A = 0.36$ to symmetric composition $\bar{f}_A = 0.5$. The results are similar to Fig. 2 when the number of blending long chain length is equal to that of short one. In particular, note that $(\chi N)_{ODT}$… between PDI_A=1.40 and 1.70 in Fig. 3c for $p_1 \neq p_2$ indeed increases as PDI in the majority component increases, confirming that the increased $(\chi N)_{ODT}$ data in Fig. 2(c) for $p_1 = p_2 = 0.5$ are not occasionally observed.

As mentioned above, DSCFT can be used to simulate the rheological measurement, which is very sensitive to detect the ODT. We investigate individual contributions of two different chains to the moduli including G'_{total}, $G'_{short\ chain}$ and $G'_{long\ chain}$ with variation in PDI_A for more detailed insights in chain length effects on $(\chi N)_{ODT}$. Fig. 4 shows the simulated temperature sweep of moduli G' of polydisperse majority block such as $\bar{f}_A = 0.64$ in Fig. 3c. In this case, majority A species form the matrix while minority B forms micellar phase, with corresponding blending information of two kinds of different chain lengths in Table 1. In the case of Fig. 4a–c, $(\chi N)_{ODT}$ decreases as the PDI_A increases in Fig. 3c, while Fig. 4d and e corresponds to the reverse case that $(\chi N)_{ODT}$ increases as the PDI_A increases in Fig. 3c. In Fig. 4a–c, long chains in the majority domain sustain the phase-separated domain while short chains can effectively fill the system space. This will lead to the decrease in $(\chi N)_{ODT}$ with the increase in PDI_A, which is similar to the case of polydisperse minority. Comparing the segment density in Fig. 4a–c, the longer chain N_1 takes the priority in the system with the composition ratio f_{N1}:f_{N2}=1.6 in Fig. 4a, f_{N1}:f_{N2}=3.7 in Fig. 4b and f_{N1}:f_{N2}=4.0 in Fig. 4c. Moreover, as shown in Fig. 4a–c, the contribution of $G'_{long\ chain}$ dominates the ODT of the system, which means long chains N_{A1} dominate the phase behavior. On the other hand, the block length N_{A2} of short chains decreases from N_{A2}=30 in Fig. 4a to N_{A2}=10 in Fig. 4b to N_{A2}=4 in Fig. 4c. Short block chains N_{A2} can more effectively fill the system space to stabilize the phase structure, inducing the decrease in $(\chi N)_{ODT}$.

However, the situation is different between PDI_A=1.40 and 1.70 in Fig. 3c with $\bar{f}_A = 0.64$, where $(\chi N)_{ODT}$ increases with the increase in PDI_A. Comparing the segment density and chain number in Fig. 4d and e, the short chain N_2 takes the priority in the system with the density ratio f_{N1}:f_{N2}=0.46 and f_{N1}:f_{N2}=0.59, respectively. Furthermore, f_{A1}:f_{A2}=0.67 and the chain number ratio p_1:p_2=0.18 in Fig. 4d and f_{A1}:f_{A2}=0.91 and p_1:p_2=0.20 in Fig. 4e according to Table 1. From Fig. 4d and e, it is clearly shown that the contribution of short chains $G'_{short\ chain}$ dominates $(\chi N)_{ODT}$. In this case, short chains weaken the effective potential holding the phase-separated microdomains and thus leading to the increase in $(\chi N)_{ODT}$.

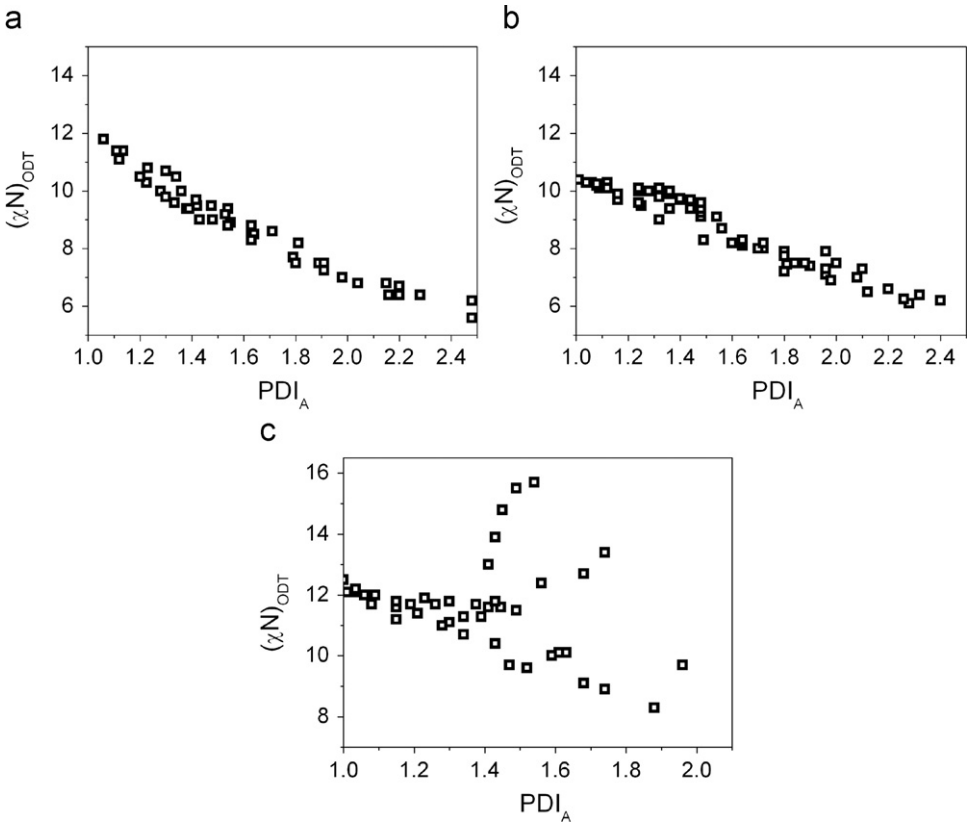

Fig. 3. Simulated $(\chi N)_{ODT}$ vs. PDI_A with random mixing number fraction ($p_1 \neq p_2$). The rheological measurement is carried out at strain amplitude Γ=0.01 and reduced frequency of ω=0.02: (a) $\bar{f}_A = 0.36$, (b) $\bar{f}_A = 0.5$ and (c) $\bar{f}_A = 0.64$.

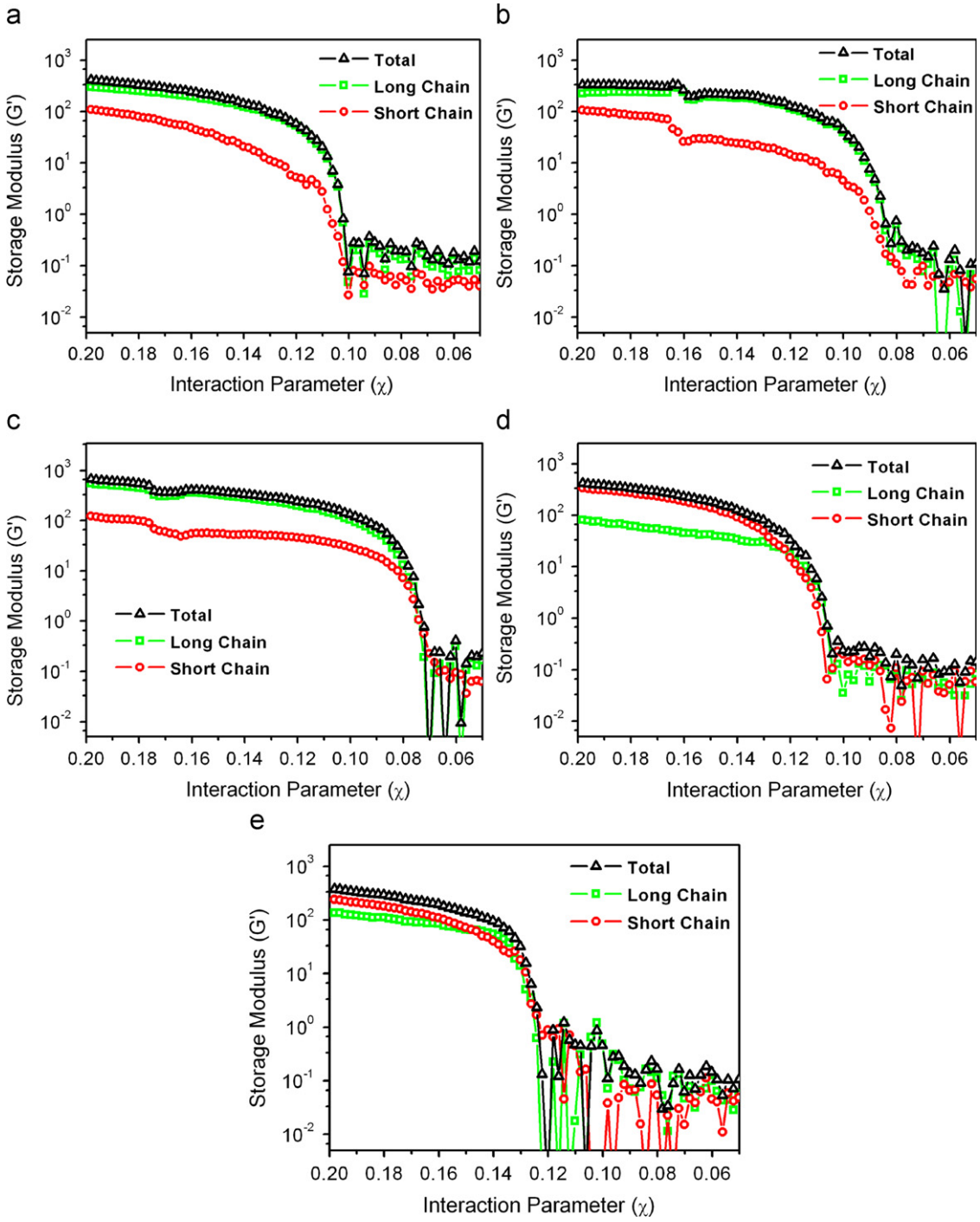

Fig. 4. Simulated $(\chi N)_{ODT}$ vs. PDI_A for $\bar{f}_A = 0.64$ blends with random mixing number fraction ($p_1 \neq p_2$). The rheological measurement is carried out at strain amplitude $\Gamma = 0.01$ and reduced frequency of $\omega = 0.02$. For the detailed blending information, see Table 1: (a) $PDI_A = 1.38$, (b) $PDI_A = 1.61$, (c) $PDI_A = 1.88$, (d) $PDI_A = 1.49$ and (e) $PDI_A = 1.68$.

Table 1
Chain length information of mixtures with different chain lengths in Fig. 4.

PDI_A	N_{A1}: N_{A2}	f_{N1}:f_{N2}	f_{A1}:f_{A2}	p_1:p_2	χN_{ODT}
(a) 1.38	$N_{A1}=110, N_{A2}=30$	1.6	2.7	0.74	11.7
(b) 1.61	$N_{A1}=110, N_{A2}=10$	3.7	12.9	1.2	9.4
(c) 1.88	$N_{A1}=124, N_{A2}=4$	4.0	31.0	1.0	8.3
(d) 1.49	$N_{A1}=170, N_{A2}=45$	0.46	0.67	0.18	11.5
(e) 1.68	$N_{A1}=180, N_{A2}=40$	0.59	0.91	0.20	12.7

4. Conclusions

In this paper, we extend the variable cell shape DSCFT, which is capable of accounting for the inhomogeneity-induced changes in the chain conformations and their coupling to the external field such as shear through the chain propagator $q(\mathbf{r},s)$, to study the effects of increase in polydispersity on the ODT in binary diblock copolymer mixtures with different chain lengths. Typically, increase in PDI in a block comprising the minority of copolymers or symmetric

composition will decrease $(\chi N)_{ODT}$. Compared to the monodisperse block copolymer, for polydisperse block copolymers, the longer chains can be less extended to the center of the microphase-separated domain to decrease entropic penalty of stretching, whereas the short chains located at the interface can minimize unfavorable contacts between unlike segments. Therefore, the effect of polydispersity due to long and short chains can fill the space efficiently favoring ordered structures, leading to lower $(\chi N)_{ODT}$ relative to the homogeneous disordered state. However, when polydispersity lies in the majority block, $(\chi N)_{ODT}$ increases with the increase in PDI at certain PDI values. When the contribution of $G'_{\text{long chain}}$ dominates the ODT of the system, long chains in the majority domain sustain the phase-separated domain while short chains can effectively fill the system space, leading to the decrease in $(\chi N)_{ODT}$ with the increase in PDI. This is similar to the case that the minority is polydispersed. However, this tendency will be reversed when short chains contribution to $G'_{\text{short chain}}$ dominates $(\chi N)_{ODT}$, as shown in Fig. 4d and e. In this case, short chains weaken the effective potential holding the phase-separated microdomains and thus leading to the increase in $(\chi N)_{ODT}$. Therefore, the location of ODT can be conveniently controlled by properly tuning the polydispersity, which does have potential applications in obtaining favorable processing conditions.

Acknowledgments

We thank for the financial support from the National Basic Research Program of China (Grant nos. 2008AA032102 and 2011CB605700). The NSF of China (Grant nos. 20990231 and 20874020) is also acknowledged.

References

[1] F.S. Bates, MRS Bull. 30 (2005) 525.
[2] D. Bendejacq, V. Ponsinet, M. Joanicot, Y.L. Loo, R.A. Register, Macromolecules 35 (2002) 6645.
[3] A.V. Ruzette, S. Tence-Girault, L. Leibler, F. Chauvin, D. Bertin, O. Guerret, P. Gerard, Macromolecules 39 (2006) 5804.
[4] N.A. Lynd, A.J. Meuler, M.A. Hillmyer, Prog. Polym. Sci. 33 (2008) 875.
[5] Y. Matsushita, A. Noro, M. Iinuma, J. Suzuki, H. Ohtani, A. Takano, Macromolecules 36 (2003) 8074.
[6] N.A. Lynd, M.A. Hillmyer, Macromolecules 38 (2005) 8803.
[7] N.A. Lynd, B.D. Hamilton, M.A. Hillmyer, J. Polym. Sci. Pt. B—Polym. Phys. 45 (2007) 3386.
[8] A.J. Meuler, C.J. Ellison, J. Qin, C.M. Evans, M.A. Hillmyer, F.S. Bates, J. Chem. Phys. 130 (2009) 234903.
[9] M.W. Matsen, Eur. Phys. J. E 21 (2006) 199.
[10] S.W. Sides, G.H. Fredrickson, J. Chem. Phys. 121 (2004) 4974.
[11] D.M. Cooke, A.C. Shi, Macromolecules 39 (2006) 6661.
[12] M.W. Matsen, Phys. Rev. Lett. 99 (2007) 148304.
[13] G.H. Fredrickson, V. Ganesan, F. Drolet, Macromolecules 35 (2002) 16.
[14] M.W. Matsen, M. Schick, Phys. Rev. Lett. 72 (1994) 2660.
[15] F. Drolet, G.H. Fredrickson, Phys. Rev. Lett. 83 (1999) 4317.
[16] N.A. Lynd, M.A. Hillmyer, Macromolecules 40 (2007) 8050.
[17] T.M. Beardsley, M.W. Matsen, Eur. Phys. J. E 27 (2008) 323.
[18] X. Li, P. Tang, H.D. Zhang, F. Qiu, Y.L. Yang, J.Chem. Phys. 128 (2008) 114901.
[19] B. Narayanan, V.A. Pryamitsyn, V. Ganesan, Macromolecules 37 (2004) 10180.
[20] J. Fraaije, J. Chem. Phys. 99 (1993) 9202.
[21] A.V. Zvelindovsky, G.J.A. Sevink, B.A.C. van Vlimmeren, N.M. Maurits, J. Fraaije, Phys. Rev. E 57 (1998) R4879.
[22] J.L. Barrat, G.H. Fredrickson, S.W. Sides, J. Phys. Chem. B 109 (2005) 6694.
[23] D. Nguyen, X. Zhong, C.E. Williams, A. Eisenberg, Macromolecules 27 (1994) 5173.
[24] A. Noro, M. Okuda, F. Odamaki, D. Kawaguchi, N. Torikai, A. Takano, Y. Matsushita, Macromolecules 39 (2006) 7654.
[25] X. Li, P. Tang, F. Qiu, H.D. Zhang, Y.L. Yang, J. Phys. Chem. B 110 (2006) 2024.
[26] G.H. Fredrickson, F.S. Bates, Annu. Rev. Mater. Sci. 26 (1996) 501.
[27] Z.L. Zhang, H.D. Zhang, Y.L. Yang, I. Vinckier, H.M. Laun, Macromolecules 34 (2001) 1416.
[28] L. Leibler, H. Benoit, Polymer 22 (1981) 195.
[29] K.M. Hong, J. Noolandi, J. Polym. Commun. 25 (1984) 265.
[30] C. Burger, W. Ruland, A.N. Semenov, Macromolecules 23 (1990) 3339.
[31] N.A. Lynd, M.A. Hillmyer, M.W. Matsen, Macromolecules 41 (2008) 4531.
[32] Y. Jiang, R. Huang, H.J. Liang, J. Chem. Phys 123 (2005) 124906.